IEEE Access
Multidisciplinary | Rapid Review | Open Access Journal

Received May 2, 2020, accepted May 15, 2020, date of publication May 19, 2020, date of current version June 2, 2020.

Digital Object Identifier 10.1109/ACCESS.2020.2995601

Prediction Method of Driving Strategy of High-Power IGBT Module Based on MEA-BP Neural Network

ZHAOLIANG MENG[1,2], YUAN YANG[1], YONG GAO [1,2], (Member, IEEE), SHENGSHENG AI[2], YUE ZHANG[2], YARU LV[2], ZETAO ZHANG[2], YANG WEN[1], LEI WU[1,3], PING ZHANG[4], AND JOHN DOUGLAS THOMSON[5]

[1]Department of Electronic Engineering, Xi'an University of Technology, Xi'an 710048, China
[2]Department of Electrical Engineering, Xi'an Polytechnic University, Xi'an 710048, China
[3]CRRC Xi'an Yongdian Electronic Company, Ltd., Xi'an 710016, China
[4]Physics Department, Anshan Normal University, Anshan 114005, China
[5]Graduate School of Business and Law, RMIT University, Melbourne, VIC 3000, Australia

Corresponding author: Yuan Yang (yangyuan@xaut.edu.cn)

This work was supported in part by the National Natural Science Foundation of China under Grant 51477138, in part by the Key Research and Development Program of Shaanxi in Shaanxi, China, under Grant 2017ZDXMGY-130, in part by the College Talent Service Enterprise Engineering under Grant 2017080CG/RC043(XALG009), and in part by the Xi'an Science and Technology Plan Project under Grant 2017074CG/RC037(XAGC009).

ABSTRACT An insulated gate bipolar transistor (IGBT) driver is crucial for improving the reliability of a power electronics system. This paper proposes a method for predicting the optimal driving strategy of high-power IGBT module based on backpropagation neural network optimized by the mind evolutionary algorithm in order to solve the problem of compromise among switching loss, switching time and overshoot and achieve a good driving effect. The three regions of switching transitions are analyzed based on the switching characteristics of the IGBT module. Neural networks are established to predict turn-on and turn-off driving strategies for variable gate resistance active gate driver of the IGBT module. The mind evolutionary algorithm is used to optimize the weights and biases of the neural networks so that the optimal weights and biases can be obtained. In order to verify the effectiveness of the driving strategy prediction method proposed in this paper, experiments are carried out for 4500V/900A the IGBT module. Compared to the conventional gate driver, the predicted driving strategies reduce the turn-on energy loss, turn-on time, over-current, comprehensive evaluation method, turn-on delay time and tail voltage duration by 59.31%, 46.38%, 36.99%, 65.65%, 1.9 μs, 2.9 μs, respectively. It was also found that the Planar-IGBT turn-off process was rarely affected by the gate resistance. The proposed method in this paper can be used not only for the guidance of the driving strategy determination of high-power the IGBT module driver, but also for the driver circuit improvement in the design process.

INDEX TERMS IGBT module, active gate driver, MEA-BP neural network, driving strategy optimization, data-driven method.

I. INTRODUCTION

The semiconductor power device insulated gate bipolar transistor (IGBT) was invented by Dr. Baliga in 1979, and since then, the IGBT have made great contributions in different fields, such as transportation, industry, lighting, consumer electronics, medical treatments, national defense, renewable energy, and power transmission [1]. The IGBT and its driver have been constantly studied and researched. Under the premise of ensuring the safety and reliability of a chip, reducing the switching loss of the device to improve the energy conversion efficiency is one of the research topics.

During design of a driver, not only the switching characteristics, switching loss, turn-off over-voltage, short-circuit safe operating area (SCSOA), reverse biased safe operating area (RBSOA), and electromagnetic interference (EMI) need to

The associate editor coordinating the review of this manuscript and approving it for publication was Zhilei Yao.

be considered, but also an optimal compromise among the switching overshoot, the switching time and the switching loss need to be achieved [2]. If the compromise problem is not handled well, there will be long switching time, large switching loss, or the module damage. In [2]–[5], active gate driver (AGD) reduced switching loss and overshoot by variable gate current. In [6]–[9], AGD reduced switching loss and overshoot by variable gate resistance. In [10]–[15], AGD reduced switching loss and overshoot by variable gate voltage. However, it was not explained how the parameters of the driving strategy should be selected to achieve the minimum switching energy loss, minimum switching time, minimum peak voltage, and minimum peak current, or comprehensive consider all aspects of the driving effect. Neither did it explain how to achieve the optimal compromise among the switching overshoot, the switching time and the switching loss.

Moreover, when designing an AGD, it is important to understand IGBT device characteristics. The IGBT module model can be used to understand the characteristics of the IGBT module. Common physical IGBT module models include the Sheng model [16], Palmer model [17], Hefner model [18]–[21], and Kraus model [22]. These models can describe the steady-state or dynamic characteristics of IGBT chips accurately. Besides, many behavioral models have been proposed [23]–[27]. When the physical model is used, it is necessary to know the internal structure of an IGBT. However, the IGBT model parameters are numerous, so the determination of parameters is very complex [28], which puts higher demands on driver design. Besides, physical models include a large number of complex differential equations, which increases both the computation burden and the simulation time [23]. Moreover, there is a problem of computational convergence, which is particularly prominent in complex multi-IGBT module circuits. In addition, in practical applications, the IGBT module integrates a fast recovery diode (FRD), and there are many parasitic parameters in the module [29]–[33], which makes the IGBT model more complex and costly.

Therefore, this paper proposes a simple method to solve the compromise problem and formulate the optimal driving strategy, while exerting the AGD optimal driving effect. With the development of big data in the information technology field, the computer-aided solutions to various problems have been promoted in many fields. Some of the machine learning-assisted methods are the computer-aided prediction of highly-selective catalysts [34], a fault prediction for vehicular networks [35], the discovery of new peptide substrates for enzymes [36], and an assistant somatic mutation detection [37]. In particular, Zeng conducted the virtual measurement of the IGBT module current using machine learning [38]. In [39], the lifetime estimation of the IGBT devices was conducted using machine learning. Also, Oukaour detected the aging defect of the IGBT power module using machine learning [40]. Machine learning-based methods have the ability to find the relationships in data needed to conduct scientific research tasks efficiently.

Therefore, this paper takes the three-stage variable gate resistance method as the research object and presents a simple prediction method of driving strategy based on backpropagation (BP) neural network optimized by the mind evolutionary algorithm (MEA). Taking switching time as a constraint condition, the compromise problem between switching loss and overshoot is solved, while achieving the minimum switching energy loss, minimum switching time, and minimum peak current, or comprehensive consider all aspects of the driving effect. The proposed method is simple and does not require knowing the internal structure and model parameters of an IGBT, and the professional requirements for designers are low, thus achieving the following:

- reduce delay time at turn-on and total turn-on time;
- reduce turn-on di_c/dt and associated reverse-recovery effects;
- lower tail voltage and turn-on energy loss;
- realize more simple turn-on and turn-off variable gate resistance driving circuit.

The rest of the paper is organized as follows. In Section II, the three-stage IGBT module switching process, conventional gate driver, and variable gate resistance method are presented in detail. Subsequently, the Prediction method of the driving strategy is introduced in Section III, and the verification test is presented in Section IV. In Section V, the analysis and discussion are provided. Finally, conclusions are given in Section VI.

II. ANALYSIS OF THE IGBT MODULE SWITCHING CHARACTERISTICS

A. THREE-STAGE IGBT MODULE SWITCHING PROCESS

In this paper, the turn-on and turn-off transitions of the IGBT module are both divided into three regions in order to obtain different control purposes based on the successive stages of the switching transient, as shown in Fig. 1. Hence, a three-stage AGD technique is improved. The three-stage turn-on transition is as follows. The turn-on stage I lasts Δt_1, that is, from the moment gate voltage v_{ge} rises from v_{goff} to the moment of the collector current i_c starts to rise. The turn-on stage II lasts Δt_2, and in this stage, the current rises from i_c to its maximum turn-on current peak I_{peak}. The turn-on stage III lasts Δt_3, and in this stage, the current decreases from I_{peak} to the end of the turn-on transition. The three-stage turn-off transition is as follows. The turn-off stage I lasts Δt_4; this stage starts from the gate voltage v_{ge} decreasing from v_{gon} till the collector current i_c starts declining. The turn-off stage II lasts Δt_5, from the moment i_c fails from I_L to the moment of the maximum turn-off voltage peak V_{peak} decreasing to bus voltage V_{dc}. Lastly, the turn-off stage III lasts Δt_6, and this stage lasts from the end of the turn-off stage II to the end of the turn-off transition.

Gate resistance R_g has an effect on the turn-on time t_{on}, the delay time at turn-on t_{don}, overshoot collector current ΔI_c, di_c/dt, turn-on energy loss E_{on}, turn-off time t_{off}, the delay time at turn-off t_{doff}, overshoot collector-emitter voltage

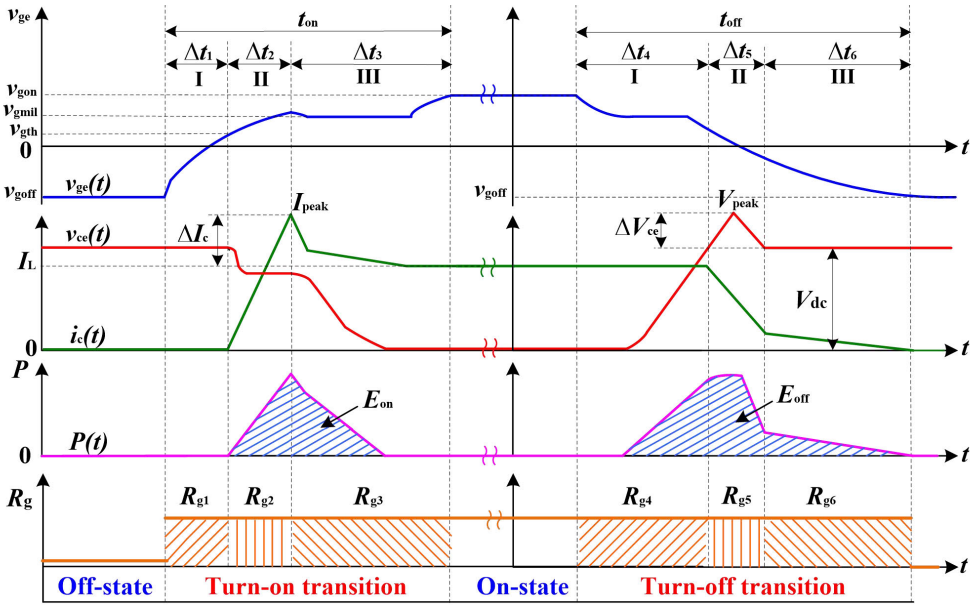

FIGURE 1. The turn-on and turn-off waveforms of an IGBT module.

ΔV_{ce}, dv_{ce}/dt, and turn-off energy loss E_{off} [9]. The greater the gate resistance is, the more switching time and switching loss increase, while overshoot decreases. The turn-on time t_{on} and ΔI_c are respectively expressed as:

$$t_{on} = \Delta t_1 + \Delta t_2 + \Delta t_3 \tag{1}$$

$$\Delta I_c = I_{peak} - I_L \tag{2}$$

where I_L denotes the rated current of an IGBT module. Further, the turn-on energy loss E_{on} is given by:

$$E_{on} = \int_0^{t_{on}} v_{ce}(t) i_c(t) dt \tag{3}$$

where $v_{ce}(t)$ denotes the collector-emitter voltage, and $i_c(t)$ represents the collector current. The turn-off time t_{off}, ΔV_{ce}, and turn-off energy loss E_{off} are respectively expressed as:

$$t_{off} = \Delta t_4 + \Delta t_5 + \Delta t_6 \tag{4}$$

$$\Delta V_{ce} = V_{peak} - V_{dc} \tag{5}$$

$$E_{off} = \int_0^{t_{off}} v_{ce}(t) i_c(t) dt \tag{6}$$

B. CONVENTIONAL GATE DRIVER

The operation principles of turn-on and turn-off circuits of conventional gate driver (CGD) are shown in Figs. 2(a) and 2(b), respectively [41]. In Fig. 2, Q_1 and Q_2 represent MOSFETs, and R_{gon} and R_{goff} represents gate resistances. In Fig 2(a), in turn-on transition, Q_1 and R_{on} are used. In Fig 2(b), in turn-off transition, Q_2 and R_{goff} are used.

C. VARIABLE GATE RESISTANCE METHOD

The schematic of a three-stage variable gate resistance driver circuit is shown in Fig. 3. In Fig. 3, Q_1-Q_6 represent MOS-

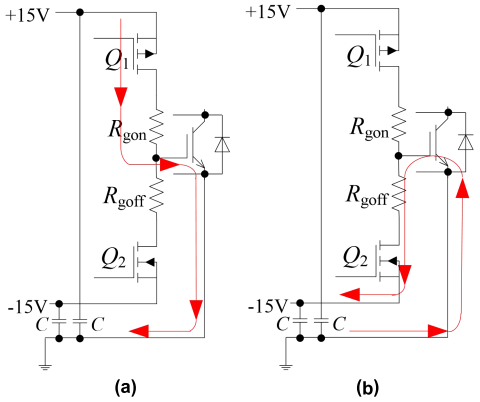

FIGURE 2. The operation principles of the CGD. (a) Turn-on transition. (b) Turn-off transition.

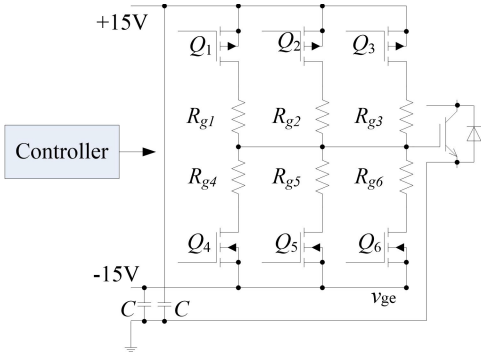

FIGURE 3. The variable gate resistance driver circuit.

FETs, and R_{g1}-R_{g6} represents gate resistances. Gate resistances R_{g1}, R_{g2}, and R_{g3} are used in the three stages of the turn-on transition, respectively; and gate resistances R_{g4}, R_{g5}, and R_{g6} are used in the three stages of the turn-off transition, respectively. As previously mentioned, the driving strategy is determined by the MEA-BP neural network prediction

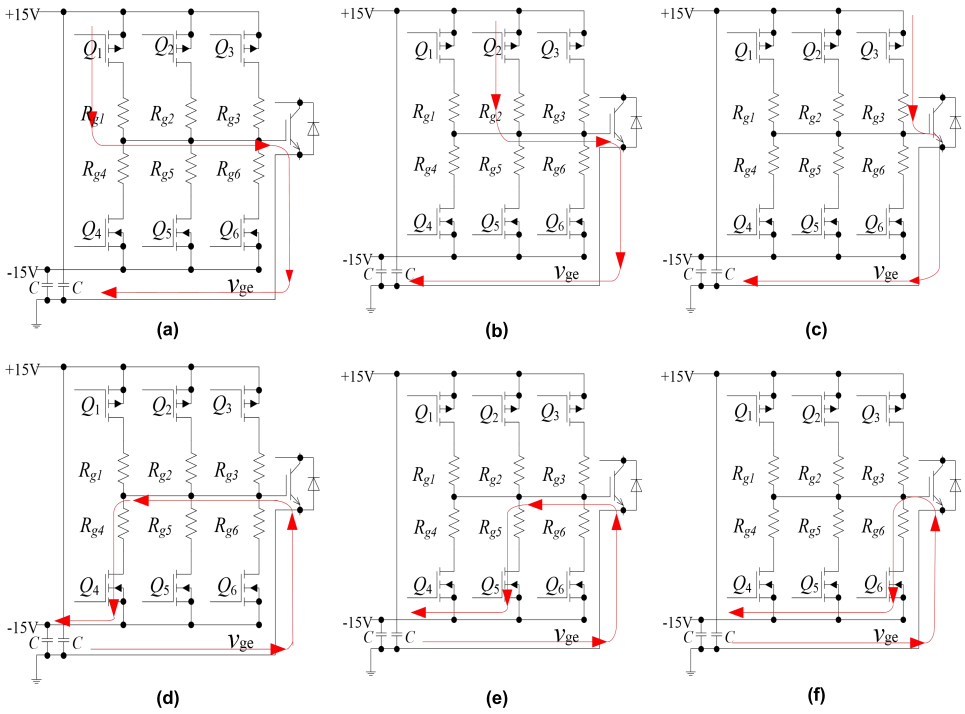

FIGURE 4. The operation principles of the three-stage switching circuit. (a) Turn-on stage I. (b) Turn-on stage II. (c) Turn-on stage III. (d) Turn-off stage I. (e) Turn-off stage II. (f) Turn-off stage III.

model. Then, according to the driving strategy, the controller complex programmable logic device (CPLD) controls Q_1-Q_6 to realize the driving of the IGBT module.

The operation principles of the three stages of the turn-on circuit are shown in Figs. 4(a)-4(c), respectively, and the operation principles of the three stages of the turn-off circuit are shown in Figs. 4(d)-4(f), respectively. On the one hand, in turn-on stage I, Q_1 and R_{g1} are used, in turn-on stage II, Q_2 and R_{g2} are used, and in turn-on stage III, Q_3 and R_{g3} are used. On the other hand, in turn-off stage I, Q_4 and R_{g4} are used, in turn-off stage II, Q_5 and R_{g5} are used, and in turn-off stage III, Q_6 and R_{g6} are used. The variable gate resistance method is simply to improve t_{on}, t_{don}, ΔI_c, di_c/dt, E_{on}, t_{off}, t_{doff}, ΔV_{ce}, dv_{ce}/dt, and E_{off} using resistors with different resistance values in the three regions of turn-on and turn-off transitions. There is a complex nonlinear relationship between variable gate resistance and driving effect of the IGBT. Therefore, the variable gate resistance and driving effect of the IGBT were predicted by the neural network prediction model because it is suitable for nonlinear modeling. In this paper, the variable gate resistance method uses t_{on} as a constraint condition to make both E_{on} and ΔI_c smaller without increasing the value of t_{on}. The improvement in ΔI_c by the variable gate resistance method denoted the improvements in I_{peak} and di_c/dt. In the same way, this method uses t_{off} as a constraint condition to decrease both E_{off} and ΔV_{ce} without increasing the value of t_{off}. The improvement in ΔV_{ce} by the variable gate resistance method is improvements in V_{peak} and dv_{ce}/dt.

III. PREDICTION METHOD

The proposed method is data-driven, and it is intended to help designers improve the variable gate resistance driving method of the IGBT module. This method operates in five steps. The first step is to load the IGBT module double pulse test data. The second step is to preprocess and normalize the data. The third step is to create the neural network first, and then the data is used to train the neural network, generating the network prediction model. In order to reduce the cost of program running time, in the fourth step, the network prediction model is used to traverse the whole region with a large step to find out the region that satisfies a certain condition better than conventional gate driver, thus reducing the solution region. Lastly, in the fifth step, the network prediction model is used to traverse the solution region with a small step to find the optimal driving strategy in the solution region.

A. DOUBLE PULSE TEST DATA

In order to capture the data of the power semiconductor devices related to the IGBT module switch processes, which is then used to create the prediction model, the double pulse test was conducted to generate the data samples of the IGBT module. The double pulse test circuit is shown in Fig. 5(a). The power devices used in the test were 4500V/900A high-power IGBT modules (CM900HG-90H) from Mitsubishi. A film capacitor acted as a DC bus support capacitor. The lower IGBT served as a device under test, and an air-core inductor L served as an inductive load. The photograph of the experimental setup is shown in Fig. 5(b). The parasitic

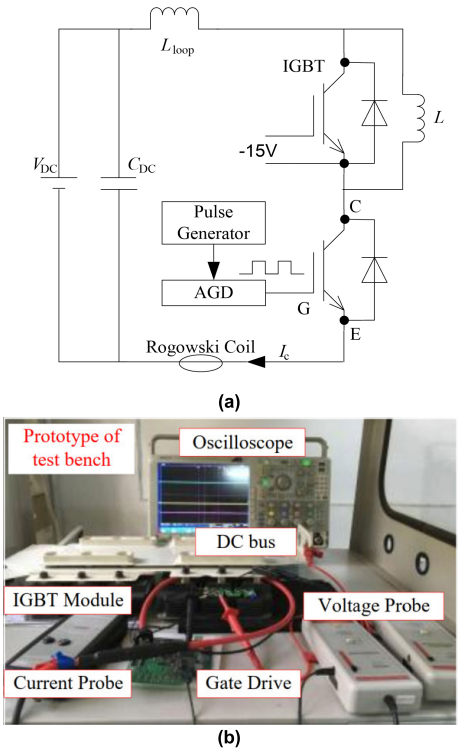

FIGURE 5. Experimental setup. (a) Double pulse test circuit diagram. (b) Photograph.

TABLE 1. Parameters of the measurement equipment and test bench.

Name	Information
Oscilloscope	Tektronix MDO4104-3,3 GHz,5 GS/s
V_{ce}	Pintech N1050B, Probe 1:100,1.5 kV/100 MHz
V_{ge}	Pintech N1050B, Probe 1:50,150 V/100 MHz
I_c	Rogowski Coil, DK-14000,0.5 mV/A,14000 A, 5 Hz-15 MHz
L	340 μH
L_{loop}	140.5 nH

inductances were measured in combination with the existing method presented in [42]. The detailed parameters of the test bench and measurement equipment are presented in Table 1.

Six resistors of 3.3 Ω, 10 Ω, 12 Ω, 16.5 Ω, 33 Ω, and 47 Ω were used as switching gate resistances. The turn-on and turn-off transitions included six stages (three stages per each transition type), and six resistances were optional in each stage; thus, there were 216 ($6 \times 6 \times 6 = 216$) groups of gate resistance combinations. The double pulse test was conducted using these 216 groups of gate resistance combinations.

B. TEST DATA PREPROCESSING AND NORMALIZATION

Because 216 groups of test data were very large, so we need to preprocess them to get the data we need. The 216 groups of test data were preprocessed to obtain t_{on}, E_{on}, ΔI_c, t_{don}, di_c/dt, t_{off}, E_{off}, ΔV_{ce}, t_{doff}, dv_{ce}/dt, and then the data were

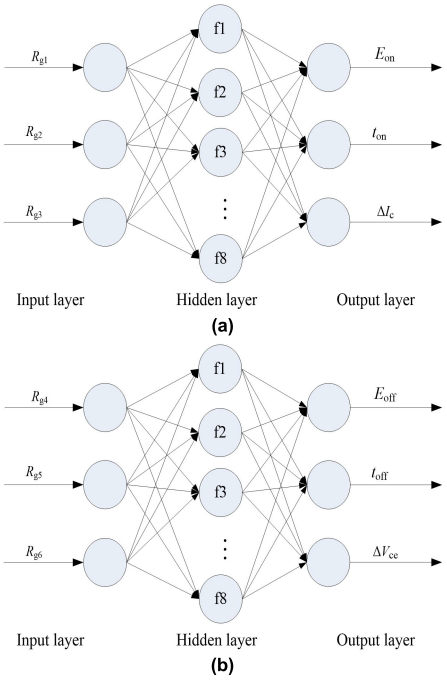

FIGURE 6. Structures of the BP neural networks: (a) turn-on prediction method; (b) turn-off prediction method.

normalized. The data were normalized by Equation 7 where x_{min} denotes the minimum value in the data sequence, and the x_{max} denotes the maximum value in the sequence.

$$x_k = \frac{x_k - x_{min}}{x_{max} - x_{min}} \tag{7}$$

C. NEURAL NETWORK DEVELOPMENT AND TRAINING

1) BP NEURAL NETWORK

The neural networks were created for the prediction of the turn-on and turn-off effects, and their structures are shown in Figs. 6(a) and 6(b), respectively. In Fig. 6, R_{g1}, R_{g2}, and R_{g3} denote the input parameters used to predict E_{on}, ΔI_c, and t_{on}; and R_{g4}, R_{g5}, and R_{g6} denote the input parameters used to predict E_{off}, ΔV_{ce}, and t_{off}. As shown in Fig. 6, the turn-on and turn-off prediction models were both three-layer neural networks, consisting of an input layer, one hidden layer, and output layer. In the input layer, there were three neurons. In the hidden layer, there were q neurons. Lastly, in the output layer, there were three neurons.

As for the connection between the input and hidden layers, w_{ij} denotes the connection weight between neuron i in the input layer and neuron j in the hidden layer, and b_j denotes the bias of neuron i. As for the connection between the hidden and output layers, v_j denotes the connection weight between two neurons from these layers, and θ denotes the neuron bias. The input of the hidden layer is given by Equation (8). As shown in Equation (9), the sigmoid function was selected

as an activation function of neurons in the hidden layer.

$$h_j = \sum_{i=1}^{3} w_{ij} R_i + b_j, \quad j = 1, 2, \ldots, q \tag{8}$$

$$z_j = f(h_j) = \frac{2}{1 + e^{-2h_j}} - 1 \tag{9}$$

The input of the output layer is given by Equation (10). As shown in equations (11), the identity function was selected as an activation function of neurons in the output layer.

$$o = \sum_{j=1}^{q} v_j z_j + \theta \tag{10}$$

$$f(o) = o \tag{11}$$

The mean squared error (MSE) and absolute error (AE) were used to evaluate the performance of the models, and they are given by Equations (12) and (13), respectively. In Equations (12) and (13), y_i denotes the actual value of the i^{th} data, y_i' denotes the value of the i^{th} data predicted by the neural network, and n is the number of samples.

$$\text{MSE} = \frac{\sum_{i=1}^{n} (y_i - y_i')^2}{n} \tag{12}$$

$$\text{AE} = \left| y_i - y_i' \right| \tag{13}$$

During the training of the BP neural network, the initial weights and biases were randomly set and adjusted according to the output error value. Namely, when the actual output cannot reach the expected value, the weights and biases are adjusted according to the error between the actual output and the expected value, until the actual output meets the expectation. Besides, the number of neurons in the hidden layer determines network nonlinearity. If the number of neurons is small, the network is under-fitting; on the contrary, a large number of neurons leads to the overfitting when the network nonlinearity is higher than that of the model itself. The number of neurons in the hidden layer is given by Equation (14), where q denotes the number of neurons in the hidden layer, N denotes the number of neurons in the input layer, M denotes the number of neurons in the output layer, m is an integer between 1 and 8. Therefore, the selection of weights and biases will be the focus of BP neural network parameters adjustment.

$$q = \sqrt{N + M} + m \tag{14}$$

2) MEA-BP NEURAL NETWORK

The mind evolutionary algorithm (MEA) was employed to optimize the BP neural network. The MEA represents the machine learning-based iterative optimization method. In the MEA, all individuals in each iteration of the evolution process are integrated into a population. A population is then divided into several subgroups. Information is exchanged between individuals and subgroups through the billboard. During the convergence process, the individuals within a subgroup compete to become winners. If there is no new winner (i.e., there is no individual with the score higher than those of the other individuals in the group), it is considered that the subgroup is mature. For a subgroup, the period from its creation to its maturity is called the life cycle. In the whole solution space, each subgroup competes to become a winner by constantly detecting new points in the solution space so as to help BP neural network obtain the optimal weights and biases [43]. The flowchart of the BP neural network where the MEA is employed for parameter optimization is shown in Fig. 7. In Fig. 7, in the MEA part, the meaning of the symbols is as follows: S_{Gi} denotes the i^{th} subgroup size, N_G denotes the number of subgroups that exist simultaneously in the algorithm; r denotes the proportion of choice in the dissimilation operation, N_R denotes the number of subgroups to be released or the number of subgroups to be created; S_R denotes the number of individuals released, t_i denotes the iteration time of the i^{th} subgroup; lastly, $c_i^{t_i}$ implies the i^{th} subgroup is at the center of the t^{th} iteration. The pseudocode of the MEA-BP algorithm is given in Algorithm 1.

Algorithm 1 MEA-BP Algorithm

Begin:
1. $N_R \leftarrow N_G$, Initialize the global billboard
2. **While** (Dissatisfy the termination conditions)
3. **If** ($N_R > 0$)
4. $r \cdot N$ individuals uniformly distributed in the solution space
5. Calculate the scores of these individuals
6. Select the best N_R individual as the initial central c_i^0 of the N_R subgroup, $N_R \leftarrow 0$, $S_R \leftarrow 0$, $t_i \leftarrow 0$
7. **end if**
8. $t_i \leftarrow t_i + 1$
9. **for** The center of each subgroup $c_i^{t_i - 1}$
10. To scatter S_{Gi} individuals around the $c_i^{t_i - 1}$ as a function of normal distribution
11. Calculate the scores of these individuals
12. Selecting the best individual from these $S_{Gi}+1$ individuals as a new center $c_i^{t_i}$ for the subgroup
13. **end for**
14. **for** Each subgroup i
15. **if** (subgroup i mature)
16. **if** (A subgroup i score better than a solution of a global billboard)
17. The local optimal solution obtained by this subgroup replaces the poor solution in the global billboard
18. **end if**
19. Release all individuals of the subgroup, $N_R \leftarrow N_R + 1$, $S_R \leftarrow S_R + S_{Gi}$, record the number of subgroups released
20. **end if**
21. **end for**
22. **end while**

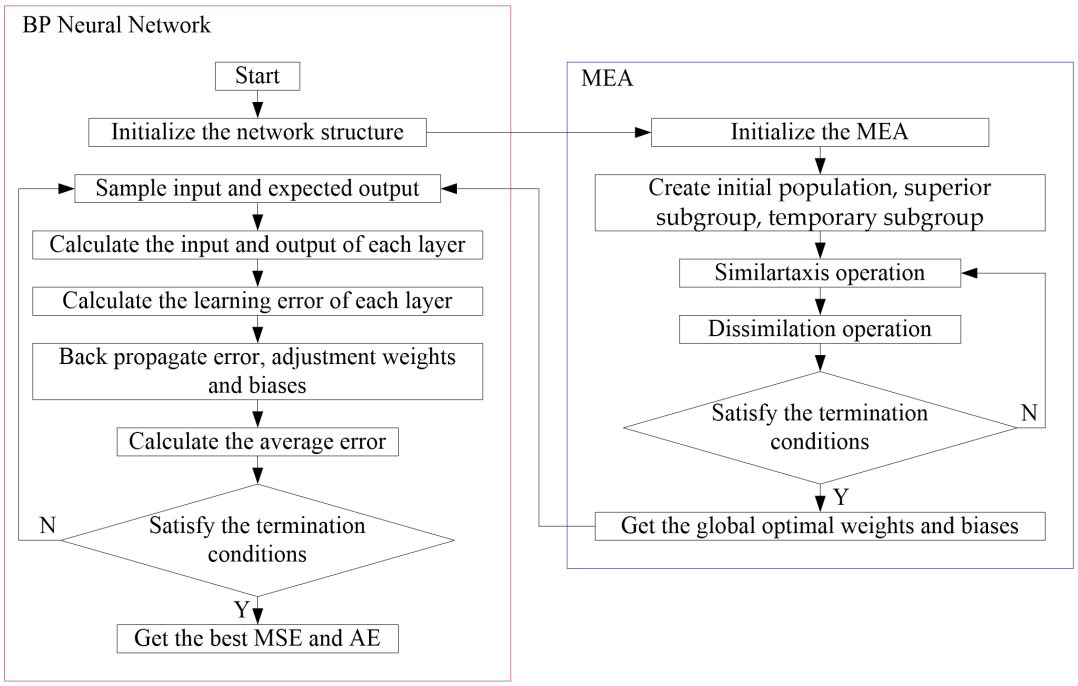

FIGURE 7. The flowchart of the MEA-BP neural network.

In the pseudocode, Steps 9-13 represent the similartaxis operation, and Steps 3-7 and Steps 14-21 represent dissimilation operation.

3) NEURAL NETWORK TRAINING

After many tests, in the MEA, there were 200 populations, five superior subgroups, and five temporary subgroups; the subgroup size was 20, and the maximal number of MEA iteration was set to ten. The hidden layer of the BP neural network contained eight neurons; the maximal number of iteration was set to 100. The MEA-BP neural network was developed using the Neural Network Toolbox of MATLAB software.

A random function was used to scramble 216 groups of test data, and then these data were divided into training and test datasets containing 151 and 65 groups, respectively. The training and test data were different in order to evaluate the generalization ability of the developed neural network prediction model, i.e., to examine whether the model can predict the results well for unknown gate driving resistance values. After the networks training, the root mean square error of turn-on neural network was found to be 1.21 e^{-12}, the root mean square error of turn-off neural network was 1.24 e^{-12}, the maximum absolute error of turn-on neural network was 4.4886 e^{-6}, and the maximum absolute error of turn-off neural network was 4.0897 e^{-6}. Figs. 8 and 9 show the best validation performance, indicating that the MSE generally improves as the number of epochs increases. In Fig. 8, it stopped after 15 epochs while the best validation performance occurred at epoch 9. In Fig. 9, it stopped after

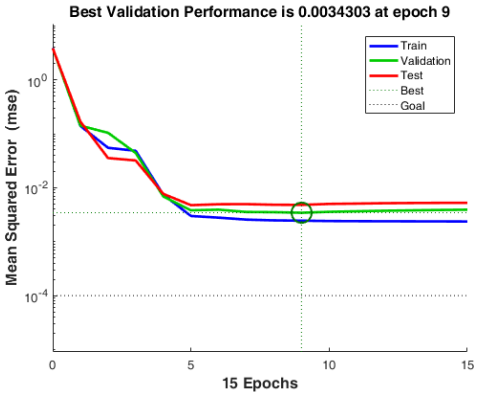

FIGURE 8. The best validation performance of turn-on prediction network.

11 epochs while the best validation performance occurred at epoch 5. The regression results are shown in Figs. 10 and 11. The relationship between the targets and outputs is measured by the correlation coefficient *RR*. The *RR* was found to be 0.98966 for the turn-on neural network, and 0.98232 for the turn-off neural network was, indicating high prediction accuracy of the network and that the network captured the relevant characteristics of the IGBT module switching process well.

D. LARGE-STEP SEGMENTATION OF SOLUTION REGION

The trained network prediction model traversed the whole region by a 1-Ω step. The relationships between gate resistance R_g and turn-on parameters are presented in Fig. 12, and the relationships between R_g and turn-off parameters are

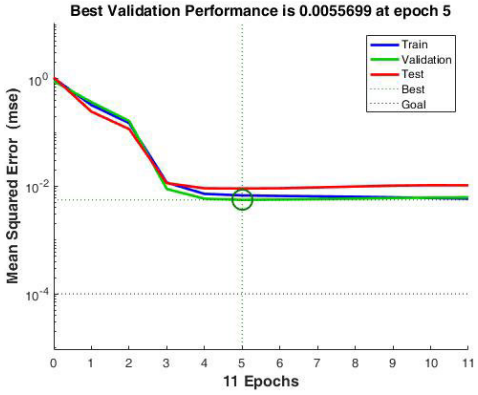

FIGURE 9. The best validation performance of turn-off prediction network.

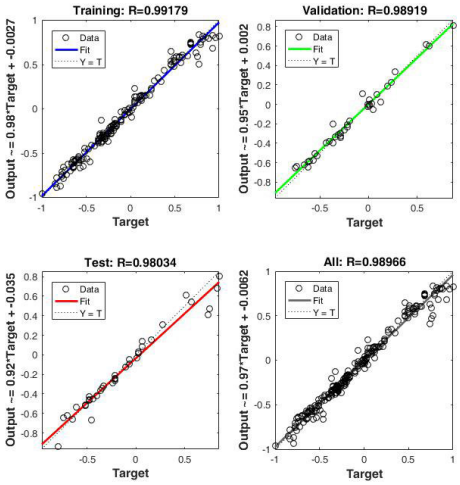

FIGURE 10. Regression of turn-on prediction network.

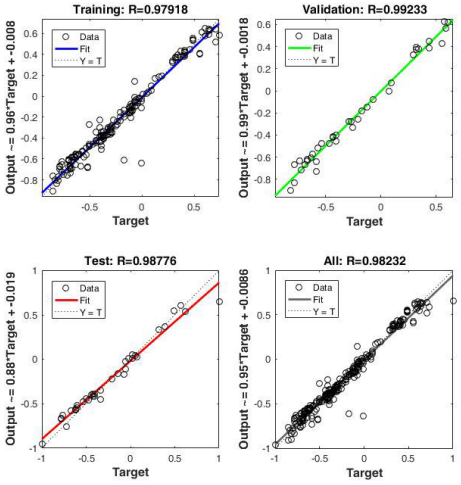

FIGURE 11. Regression of turn-off prediction network.

presented in Fig. 13. As shown in Fig. 12, turn-on energy loss E_{on} was in the range of 2-12 J, R_{g1} had little effect on E_{on}, and E_{on} increased with the increase in the values of R_{g2} and R_{g3}; the value of turn-on time t_{on} was in the range of 2-20 μs, and it increased with the increase in the three resistances. The value of ΔI_c was in the range of 200-800 A; the smaller R_{g2} was, the larger ΔI_c was. Further, R_{g1} and R_{g3} had little effect on ΔI_c, which was consistent with the operational theory of the IGBT module. As shown in Fig. 13, turn-off energy loss E_{off} was in the range of 1.6-1.72 J, and R_{g4}, R_{g5}, and R_{g6} had little effect on E_{off}; turn-off time t_{off} was in the range of 3-3.4 μs, and R_{g4}, R_{g5}, and R_{g6} also had little effect on t_{off}. Lastly, ΔV_{ce} was in the range of 620-700 V, and R_{g4}, R_{g5}, and R_{g6} had little effect on ΔV_{ce}. The results clearly present the influence of variable gate resistance on the relevant characteristics of the IGBT module. In the turn-off process, with the changes in R_g, the ranges of E_{off}, t_{off}, and ΔV_{ce} were small.

The trained network prediction model runs for a long time if the optimal driver strategy is found in the whole region. Therefore, we reduced the solution region based on the driving effect of the CGD. The driving effect of the CGD is shown in Fig. 14. In Fig. 14(a), the radar map of the CGD turn-on transition driving effect (E_{on}, ΔI_c, di_c/dt, t_{on}, t_{don}) is presented, and in Fig. 14(b), the radar map of the CGD turn-off transition driving effect (E_{off}, ΔV_{ce}, dv_{ce}/dt, t_{off}, t_{doff}) is presented. The trained prediction model traversed the whole region, and the region with the driving effect better than that of the CGD was kept, and the region with the driving inferior to the effect of the CGD was eliminated. Namely, each index of the AGD should be better than that of each index of the CGD; for instance, E_{on} of the AGD should be smaller than or equal to E_{on} of the CGD. The evaluation method based on the radar map of the driving effect presented in Fig. 14 is called the comprehensive evaluation method (CEM).

Then, the solution region reduced, as shown in Fig. 15 and Fig. 16. As shown in Fig. 15, E_{on} was in the range of 2.3 - 3.65 J, turn-on time t_{on} was in the range of 4 - 7 μs, and ΔI_c was in the range of 236-580 A. Further, as presented in Fig. 16, E_{off} was in the range of 1.6-1.72 J, t_{off} was in the range of 3-3.4 μs, and ΔV_{ce} was in the range of 620-700 V.

E. SMALL-STEP OPTIMIZING OF DRIVING STRATEGY

According to the results presented in Figs. 15 and 16, the network prediction model found out the driving strategies of the AGD using a small step of 0.1 Ω, and the corresponding distribution maps of the driving strategies are drawn in Fig. 17. In Figs. 17(a) and 17(b), there are three parts, the first part represents the variable gate resistance results of stage I, the second part represents the variable gate resistance results of stage II, and the third part represents the variable gate resistance results of stage III.

In Fig. 17, the ordinate denotes the resistance value, and the abscissa denotes the time. The turn-on strategies are shown in Fig. 17(a), where it can be seen that the resistance ranges of stage I, stage II, and stage III were 3.3-13 Ω, 3.3-39 Ω, and 3.3-15 Ω. Also, the larger the resistance was, the greater the corresponding time was. The turn-off strategies are shown in Fig. 17(b), where it can be seen that the resistance ranges

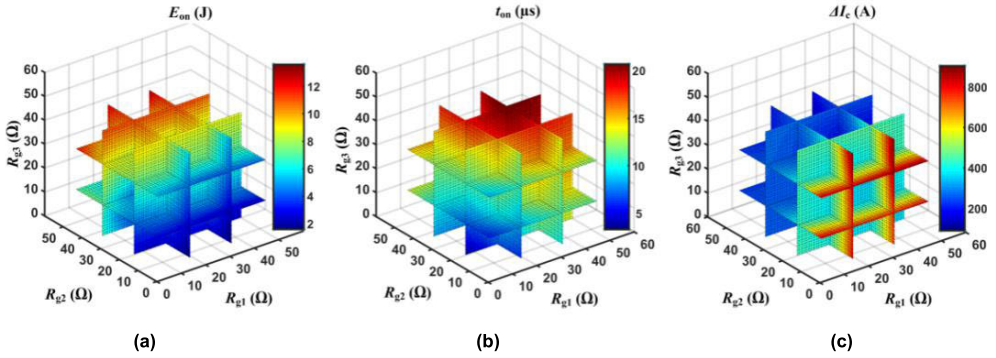

FIGURE 12. Relationships between gate resistance R_g and turn-on parameters. (a) E_{on}. (b) t_{on}. (c) ΔI_c.

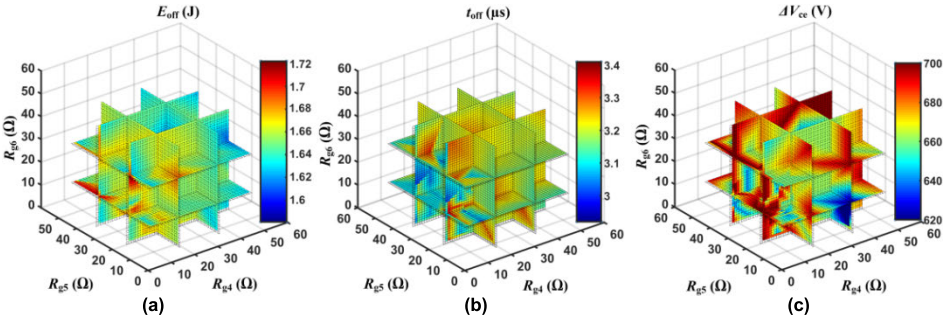

FIGURE 13. Relationships between gate resistance R_g and turn-off parameters. (a) E_{off}. (b) t_{off}. (c) ΔV_{ce}.

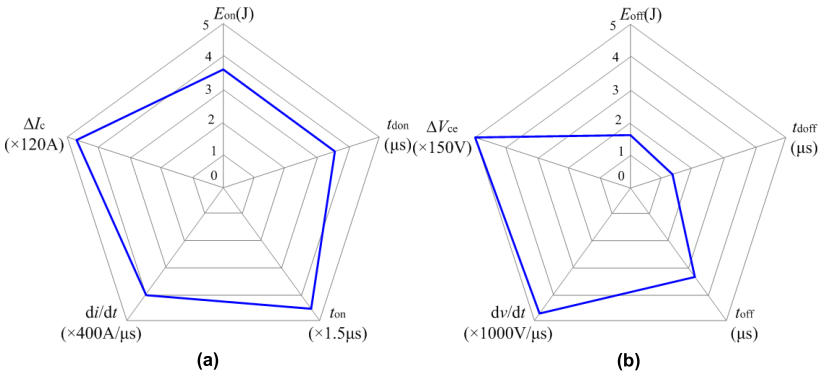

FIGURE 14. The radar map of the CGD driving effect. (a) Turn-on driving effect. (b) Turn-off driving effect.

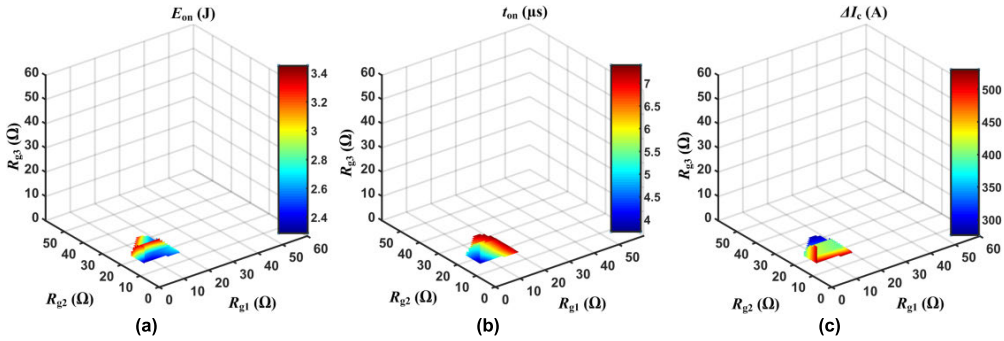

FIGURE 15. The turn-on datasets superior to the CGD. (a) E_{on}. (b) t_{on}. (c) ΔI_c.

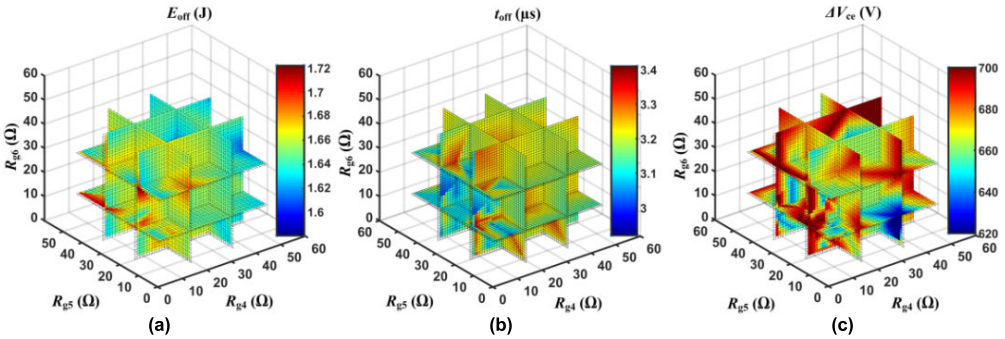

FIGURE 16. The turn-off datasets superior to the CGD. (a) E_{off}. (b) t_{off}. (c) ΔV_{ce}.

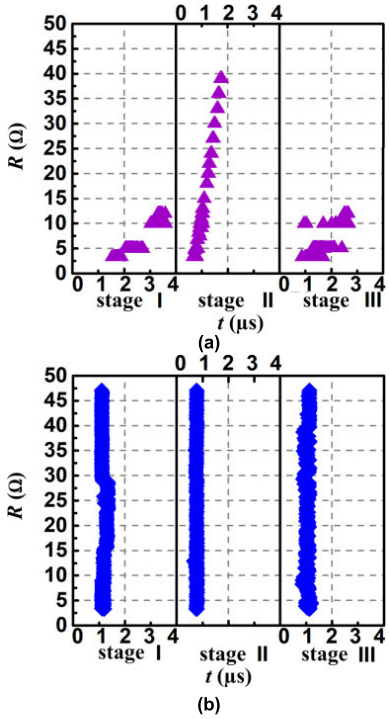

FIGURE 17. Distribution diagram of the turn-on and turn-off strategies. (a) Turn-on strategies. (b) Turn-off strategies.

of all the three stages were the same and equal to 3.3-47 Ω. Namely, with the increase in the resistance, the corresponding time was almost unchanged, and there was no trend similar to that in Fig. 17(a). The times corresponding to all the resistor ranges of the three stages were basically the same. In Fig. 17, we can identify four strategies that are based on: 1) minimum E_{on} or E_{off}, 2) minimum t_{on} or t_{off}, 3) minimum ΔI_c or ΔV_{ce}, and 4) CEM driving strategy. In order to balance the driving effect, an optimal compromise between the switching over-voltage, over-current, and the switching loss, should be achieved. The CEM driving strategy refers to the strategy of the minimum area formed by the driving effect in a radar map. The area formed by the driving effect in a radar map can be

TABLE 2. Turn-on driving strategy.

	Driving strategy method
Minimum E_{on}	R_{g1} : 3.3 Ω, R_{g2} : 13 Ω, R_{g3} : 3.3 Ω;
	Δt_1 : 1.68 μs, Δt_2 : 0.99 μs, Δt_3 : 1.06 μs.
Minimum t_{on}	R_{g1} : 3.3 Ω, R_{g2} : 13 Ω, R_{g3} : 3.3 Ω;
	Δt_1 : 1.68 μs, Δt_2 : 0.99 μs, Δt_3 : 1.06 μs.
Minimum ΔI_c	R_{g1} : 3.3 Ω, R_{g2} : 39 Ω, R_{g3} : 3.3 Ω;
	Δt_1 : 1.68 μs, Δt_2: 2.01 μs, Δt_3 : 1.99 μs.
CEM	R_{g1} : 3.3 Ω, R_{g2} : 37 Ω, R_{g3} : 3.3 Ω;
	Δt_1 : 1.68 μs, Δt_2 : 1.1 μs, Δt_3 : 1.02 μs.

calculated by:

$$S = \sum_{i=1}^{5} \frac{a_i a_{i+1} \sin \alpha}{2}, \quad a_1 = a_6 \tag{15}$$

where α is 72°, and a_i is the coordinate value in the radar map. In the ideal situation, the IGBT switching process is completed in an instant, there is not switching energy loss, and there is no switching time, that is, the driving effect of the ideal IGBT is the center point of the radar map. So the smaller the area is, the closer the situation to the ideal situation will be, and all of the parameters will be more balanced. The neural network prediction model helped us identify these four strategies and provided variable gate resistance strategies, turn-on time t_{on} and turn-off time t_{off}, so that Δt_1, Δt_2, Δt_3 could be easily obtained by the double pulse test. Take the CEM driving strategy as an example. In Step 1, the resistance of 3.3 Ω was used as a gate resistance to drive the IGBT module, and Δt_1 was obtained using the test data. In Step 2: the resistance of 3.3 Ω and Δt_1 were used as the turn-on stage I driving strategy, and then a 37 Ω resistance was used in Stage II and III, and Δt_2 was obtained using the test data. Finally, $\Delta t_3 = t_{on} - \Delta t_1 - \Delta t_2$.

The results of the turn-on and turn-off strategies are shown in Table 2 and Table 3, respectively. It should be noted that the strategies based on minimum E_{on} and minimum t_{on} provided the same results, as presented in Table 2. The turn-off strategies provided are all the same results, are presented in Table 3.

TABLE 3. Turn-off driving strategy.

Strategy type	Driving strategy method
Minimum E_{off}	R_{g4}, R_{g5}, R_{g6} were all 10 Ω; t_{off} was 3.39 μs.
Minimum t_{off}	R_{g4}, R_{g5}, R_{g6} were all 10 Ω; t_{off} was 3.39 μs.
Minimum ΔV_{ce}	R_{g4}, R_{g5}, R_{g6} were all 10 Ω; t_{off} was 3.39 μs.
CEM	R_{g4}, R_{g5}, R_{g6} were all 10 Ω; t_{off} was 3.39 μs.

IV. EXPERIMENTAL VERIFICATION

In order to evaluate the performance of the proposed strategy obtained by the MEA-BP neural network-based prediction model, the experiments were conducted. As already mentioned, the experimental platform is shown in Fig. 5, and the detailed parameters of the test bench and measurement equipment used in the test are presented in Table 1.

A. TURN-ON STRATEGY VERIFICATION

In order to verify the feasibility of the proposed AGD, the DC bus voltage was 2800 V, and the switched current was 900 A. The experimental turn-on waveforms of the IGBT module obtained by the proposed AGD are presented in Fig. 18. The experimental turn-on radar map is presented in Fig. 19, where it can be seen that the driving effect of the proposed AGD was better than that of the CGD. The driving effects of different AGD strategies were different. The values of ΔI_c, $\mathrm{d}i_c/\mathrm{d}t$, $t_{d\mathrm{on}}$, t_{on}, and E_{on} of three AGD methods were all lower than those of the CGD. Compared to the CGD, the AGD reduced the value of $t_{d\mathrm{on}}$ and tail voltage duration by 1.9 μs and 2.9 μs, respectively. On the one hand, E_{on} and t_{on} of the strategies based on minimum E_{on} and minimum t_{on} were the smallest. On the other hand, ΔI_c of the strategy based on minimum ΔI_c was the smallest. Lastly, the driving effect of the CEM was more balanced than other strategies.

More turn-on waveforms of the IGBT module under different operation temperatures are shown in Fig. 20. In the experiment of different operation temperatures, the DC bus voltage was 2800 V and the switched current was 900 A. All these parameters are consistent with 25°. It can be seen from Fig. 20 that the impact of the operation temperature on the voltage and current slopes is limited since the performance of the IGBT module varies little with different operation temperature, except that the I_{peak} changed obviously. The higher the operation temperature, the lower the I_{peak}. In addition, the turn-on delay time varies little with temperature. Therefore, the performance of the AGD will not be affected under different operation temperatures.

B. TURN-OFF STRATEGY VERIFICATION

As presented in Table 3, in the turn-off strategy obtained by the MEA-BP neural network-based prediction model, all resistances were 10 Ω. In order to verify the accuracy of the

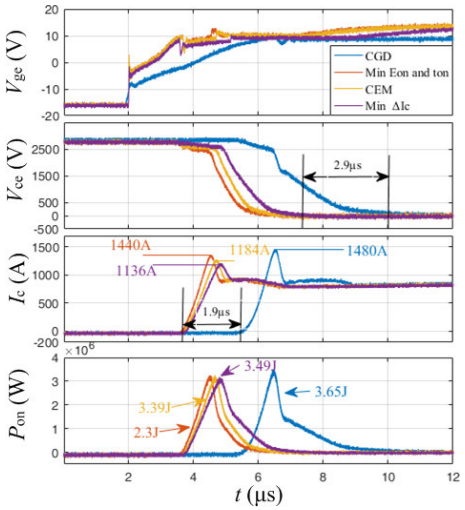

FIGURE 18. Experimental turn-on waveforms of the IGBT module.

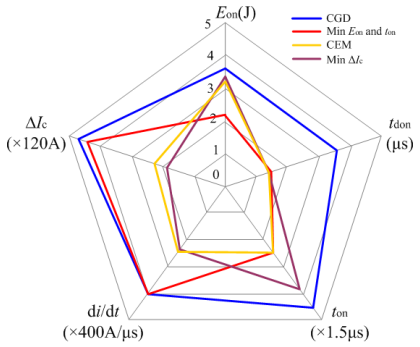

FIGURE 19. Experimental radar maps of the turn-on driving effect.

MEA-BP neural network, six driving strategies were chosen. In the first strategy (called AGD I), R_{g4} was 3.3 Ω, R_{g5} was 13 Ω, and R_{g6} was 3.3 Ω. In the second strategy (called AGD II), R_{g4} was 3.3 Ω, R_{g5} was 37 Ω, and R_{g6} was 3.3 Ω. In the third strategy (called AGD III), R_{g4} was 3.3 Ω, R_{g5} was 39 Ω, and R_{g6} was 3.3 Ω. In the fourth strategy, the gate resistance was 3.3 Ω. In the fifth strategy, the gate resistance was 16.5 Ω. Lastly, in the sixth strategy, the gate resistance was 47 Ω. The experimental verification was carried out at the DC bus voltage of 2800 V and the switched current of 900 A. The experimental turn-off waveforms of the IGBT module are presented in Fig. 21. The experimental turn-off radar map of the IGBT module is presented in Fig. 22, where it can be seen that when the gate resistance changed, the turn-off effects of six driving strategies were the same as that of the CGD; thus, the turn-off result predicted by the MEA-BP neural network prediction model was correct, and there was no need to use the variable gate resistance method during the turn-off transition.

The turn-off waveforms of the IGBT module under different operation temperatures is shown in Fig. 23. The DC bus voltage was 2800 V and the switched current was 900 A. According to the turn-off strategy obtained by the prediction model, the gate resistance was 10 Ω. In the tests conducted at different temperatures, the turn-off delay time increases as the operation temperature rises, while the voltage and current slopes maintain almost constant. Similar to the turn-on

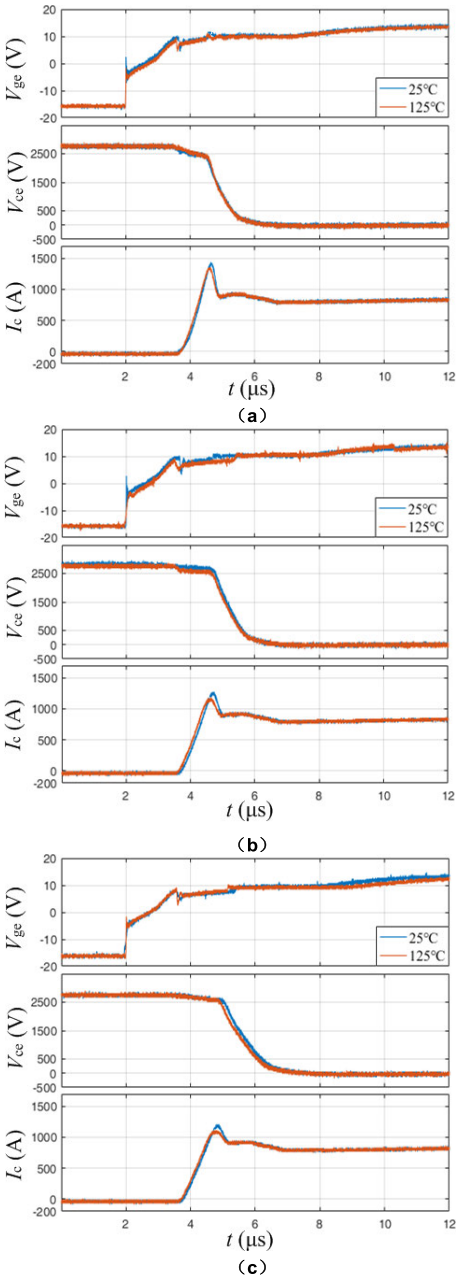

FIGURE 20. Turn-on performance comparison of the IGBT module under different operation temperatures. (a) Min E_{on} strategy. (b) CEM strategy. (c) Min ΔI_C strategy.

transient, only the V_{peak} changed obviously under different operation temperatures. The higher the operation temperature, the lower the V_{peak}. However, the performance of the turn-off strategy will not be affected under different operation temperatures since the gate resistance did not change during turn-off.

V. ANALYSIS AND DISCUSSION

Adding a suitable gate capacitance C_{ge} to the driver circuit can improve the driving effect, but this is not studies in this work. Namely, we compared the AGD and CGD without adding C_{ge}. Since C_{ge} was added to the AGD, the driving

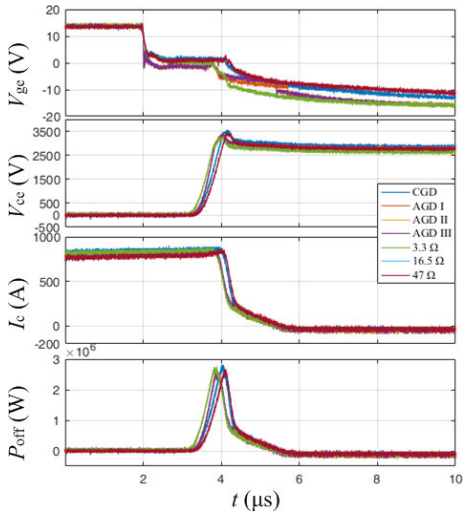

FIGURE 21. Experimental turn-off waveforms of the IGBT module.

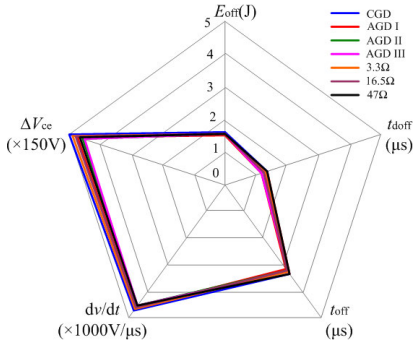

FIGURE 22. Experimental radar maps of the turn-off driving effect.

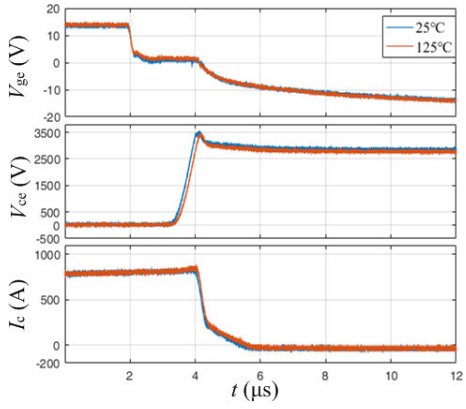

FIGURE 23. Turn-off performance comparison of IGBT module under different operation temperatures.

effect of the driving strategy predicted by the MEA-BP neural network could not be clearly determined.

A. PREDICTION ACCURACY ANALYSIS

The prediction accuracy of the MEA-BP neural network is very important. The predicted and experimental turn-on results are presented in Fig. 24, where it can be seen that there

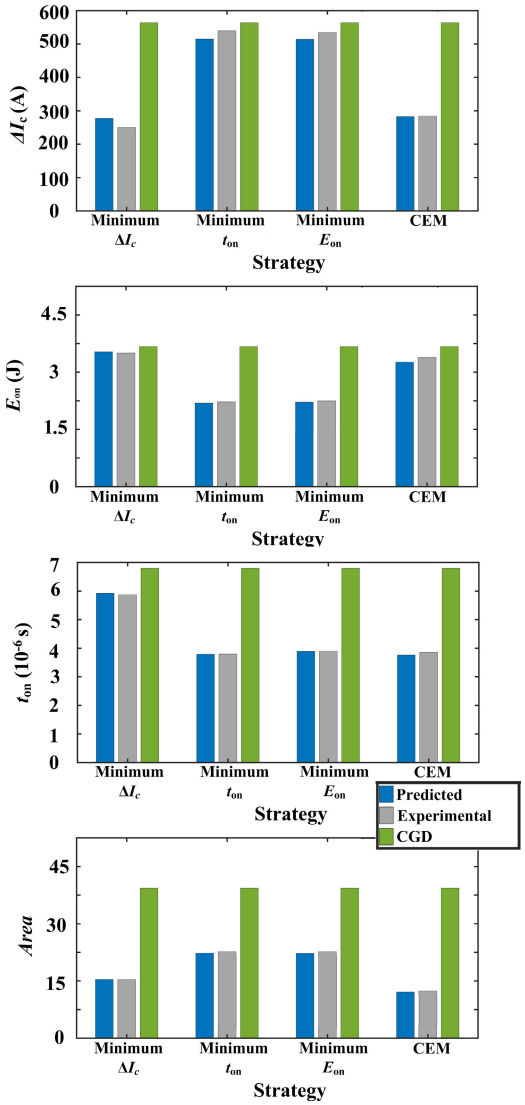

FIGURE 24. Comparison of E_{on}, t_{on}, ΔI_c, and CEM data of the turn-on process.

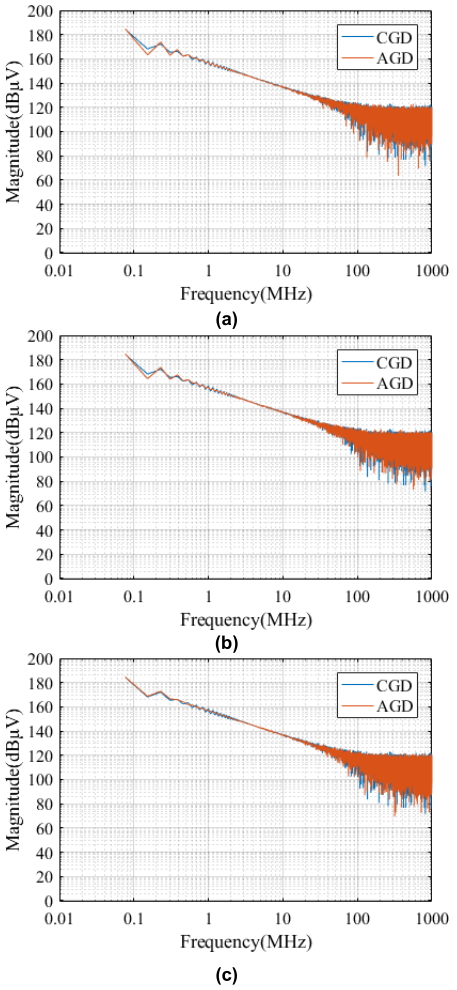

FIGURE 25. Spectrum comparison between CGD and AGD for V_{ce} experimental results. (a) Minimum E_{on} and t_{on} strategy. (b) CEM strategy. (c) Minimum ΔI_c strategy.

were small differences between the predicted and experimental results. According to the obtained results, the improvement was significant, namely:

- ΔI_c of the strategy based on minimum ΔI_c was 59.31% smaller than that of the CGD.
- t_{on} of the strategy based on minimum t_{on} was 46.38% less than that of the CGD.
- E_{on} of the strategy based on minimum E_{on} was 36.99% smaller than that of the CGD.
- the driving effect of the CEM driving strategy was 65.65% smaller than that of the CGD.

In Fig. 21, the over-voltage (V_{peak}) is determined using the stray inductance L_s and di_c/dt as follows:

$$V_{peak} = V_{dc} + L_s \cdot \left| \frac{di_c}{dt} \right| \tag{16}$$

As shown in Fig. 21, di_c/dt values of seven driving strategies were almost the same as that of the CGD, so V_{peak} values were also almost the same. In Fig. 22, it can be seen that the turn-off results predicted by MEA-BP neural network were accurate. The driving effect at a different gate resistance R_g was mostly the same.

B. ELECTROMAGNETIC INTERFERENCE ANALYSIS

In order to have an understanding of the EMI induced by high di_c/dt and dv_{ce}/dt, EMI analysis of the voltage and current waveforms were carried out, respectively. The approximation of the spectrum for both V_{ce} and I_c are shown in Figs. 25 and 26. These data were obtained by the oscilloscope Tektronix MDO4104-3 in the experiment and the spectrum was obtained applying the FFT in MATLAB software after the data were processed. The results show that the AGD did not cause additional EMI generation.

C. DRIVING STRATEGY ANALYSIS

In the turn-on transition of the IGBT module, the fast recovery diode was turning off, so the turn-on strategy was affecting

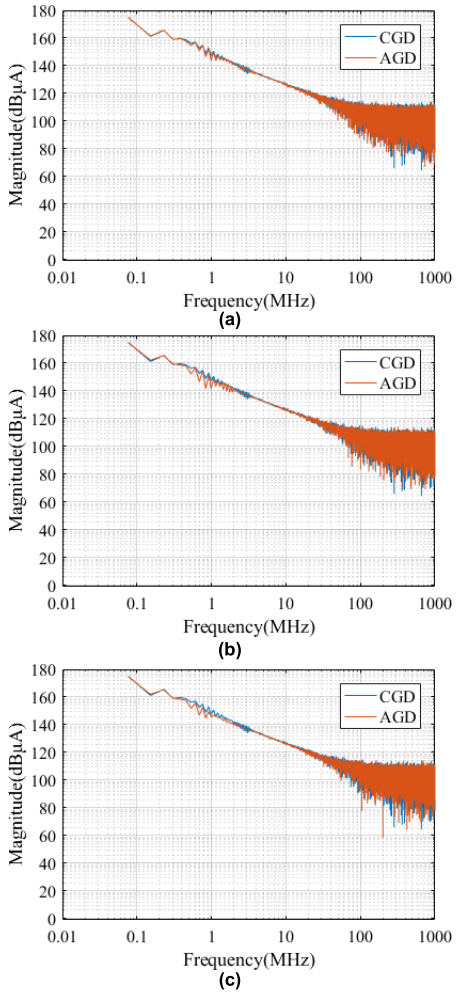

FIGURE 26. Spectrum comparison between CGD and AGD for I_c experimental results. (a) Minimum E_{on} and t_{on} strategy. (b) CEM strategy. (c) Minimum ΔI_c strategy.

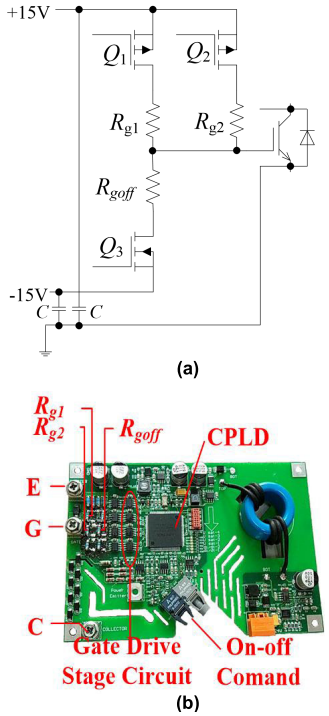

FIGURE 27. The optimized variable gate resistance method. (a) Circuit diagram. (b) Photograph.

the turn-off process of the fast recovery diode. By making the fast recovery diode turn-off softer, the loss can be reduced.

In Fig. 17(a), for the statistical turn-on strategies, it can be seen that a small resistance was used in stage I with the aim of reducing t_{don}; a large resistance was used in stage II with the aim of reducing di_c/dt and I_{peak}; and lastly, a small resistance was used in stage III, in order to make the IGBT enter the saturation region quickly.

There are two types of IGBT chips: Trench-IGBT and Planar-IGBT. The turn-off process of a Trench-IGBT is not affected by gate resistance, but the turn-off process of a Planar-IGBT is affected by gate resistance [1], [6]–[9]. The IGBT module used in this paper is the Planar-IGBT, but the turn-off strategies that are presented in Fig. 17(b) show that in the experiments, the gate resistance had little effect on the module turn-off process. The experimental results presented in Figs. 21 and 22 prove the same. After the confirmation from the chip manufacturer, it has been concluded that the IGBT chip technology has constantly been developing and that the semiconductor manufacturer had made the best optimization of the device, so there is no longer a need to improve the IGBT turn-off characteristics through the gate resistance. In Table 2, the same resistances are used for stages I and III of the turn-on strategies. Such a variable gate resistance drive circuit can be optimized in the way presented in Fig. 27(a), and the corresponding driver optimization is illustrated in Fig. 27(b). The operation principle of the three-stage turn-on circuit is shown in Fig. 28. In turn-on stages I and III, Q_1 and R_{g1} were used. Thus, due to driver optimization, the hardware cost is reduced.

VI. CONCLUSIONS AND FUTURE WORK

A prediction method of driving strategy of high-power IGBT module based on MEA-BP neural network is proposed in this paper to improve the variable gate resistance method of active gate driver. The switching process of the IGBT module is analyzed, of which the turn-on and turn-off transitions of the IGBT module are both divided into three regions in order to obtain different control purposes based on the successive stages of the switching transient. The prediction networks for turn-on and turn-off driving strategies of variable gate resistance active gate driver are established, in which the gate resistances in three-stages are input, and switching loss, switching time, overshoot are output. In order to obtain the optimal weights and biases, the mind evolutionary algorithm is used to optimize the BP neural network. The prediction method uses switching time as a constraint condition to make both switching loss and overshoot smaller without increasing the switching time. In order to verify the effectiveness of the

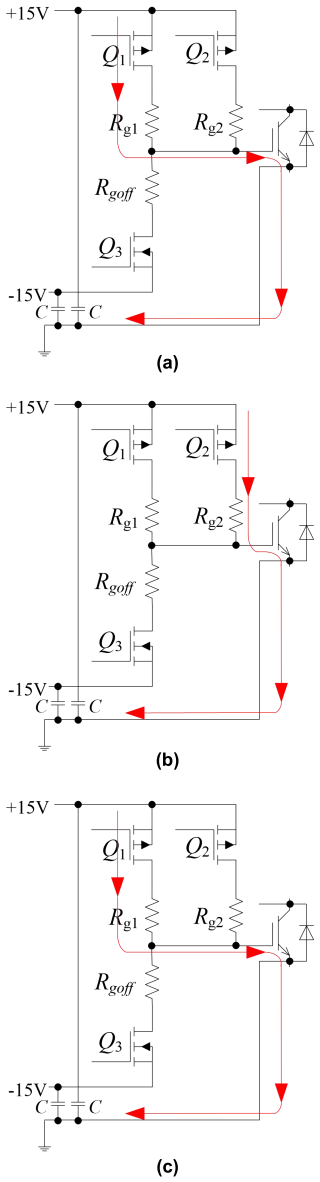

FIGURE 28. The operation principle of the optimized circuit. (a) Turn-on stage I. (b) Turn-on stage II. (c) Turn-on stage III.

driving strategy prediction method proposed in this paper, experiments are carried out for a 4500V/900A IGBT module. The experimental results show that the driving effect of the proposed driving strategies is significant. Compared to the CGD, the AGD reduces the value of $t_{d\text{on}}$ and tail voltage duration by 1.9 μs and 2.9 μs, respectively. The over-current ΔI_c of the strategy based on minimum ΔI_c is 59.31% smaller than that of the CGD. The turn-on time t_{on} of the strategy based on minimum t_{on} is 46.48% less than that of the CGD. The turn-on energy loss E_{on} of the strategy based on minimum E_{on} is 36.99% smaller than that of the CGD. Lastly, the driving effect of the CEM driving strategy is 65.65% smaller than that of the CGD.

A comprehensive evaluation method for driving effect is proposed in this paper. This method not only assists the neural network to find the optimal strategy but also determines the driving effect of the driver intuitively. It is found that the Planar-IGBT turn-off process is almost not affected by the gate resistance, which shows that due to the development of the IGBT chip technology, there is no need to use the gate resistance to improve the turn-off effect. Thus, a simpler turn-on and turn-off variable gate resistance driving circuit is realized.

A prediction method proposed in this paper is simple and versatile and can be used as a reference for further driver improvements. It can be used not only for the guidance of the driving strategy determination of high-power IGBT module driver, but also for the driver circuit improvement in the design process.

In our future work, we will use machine learning algorithms to improve the other driving methods of the IGBT and SiC MOSFET modules.

REFERENCES

[1] Baliga, B. J. *The IGBT Device: Physics, Design and Appliactions of the Insulated Gate Bipolar Transistor*. Montclair, NJ, USA: William Andrew, 2015, pp. 1–19.

[2] V. John, B.-S. Suh, and T. A. Lipo, "High-performance active gate drive for high-power IGBT's," *IEEE Trans. Ind. Appl.*, vol. 35, no. 5, pp. 1108–1117, Sep./Oct. 1999, doi: 10.1109/28.793372.

[3] G. Schmitt, R. Kennel, and J. Holtz, "Voltage gradient limitation of IGBTS by optimised gate-current profiles," in *Proc. IEEE Power Electron. Specialists Conf.*, Jun. 2008, pp. 3592–3596, doi: 10.1109/PESC.2008.4592512.

[4] J. Bauch and A. Lindemann, "Flexible switching speed control to improve switching losses and EMI by a gate driver with adjustable gate current," in *Proc. 8th Int. Conf. Integr. Power Electron. Syst.*, Nuremberg, Germany, 2014, pp. 1–6.

[5] B. Wittig and F. Fuchs, "Analysis and comparison of turn-off active gate control methods for low-voltage power MOSFETs with high current ratings," *IEEE Trans. Power Electron.*, vol. 27, no. 3, pp. 1632–1640, Mar. 2012, doi: 10.1109/TPEL.2011.2162531.

[6] R. S. Chokhawala, J. Catt, and B. R. Pelly, "Gate drive considerations for IGBT modules," *IEEE Trans. Ind. Appl.*, vol. 31, no. 3, pp. 603–611, May/Jun. 1995, doi: 10.1109/28.382122.

[7] J.-H. Kim, D.-H. Park, J.-B. Kim, and B.-H. Kwon, "An active gate drive circuit for high power inverter system to reduce turn-off spike voltage of IGBT," in *Proc. 7th Int. Conf. Power Electron.*, Daegu, South Korea, Oct. 2007, pp. 127–131, doi: 10.1109/ICPE.2007.4692362.

[8] D. Bortis, P. Steiner, J. Biela, and J. Kolar, "Double-stage gate drive circuit for parallel connected IGBT modules," *IEEE Trans. Dielectrics Electr. Insul.*, vol. 16, no. 4, pp. 1020–1027, Aug. 2009, doi: 10.1109/TDEI.2009.5211849.

[9] A. Sokolov, D. Mascarella, and G. Joos, "Variable-speed IGBT gate driver with loss/overshoot balancing for switching loss reduction," in *Proc. IEEE Energy Convers. Congr. Expo. (ECCE)*, Pittsburgh, PA, USA, Sep. 2014, pp. 1232–1239, doi: 10.1109/ECCE.2014.6953542.

[10] N. Idir, R. Bausiere, and J. J. Franchaud, "Active gate voltage control of turn-on di/dt and turn-off dv/dt in insulated gate transistors," *IEEE Trans. Power Electron.*, vol. 21, no. 4, pp. 849–855, Jul. 2006, doi: 10.1109/TPEL.2007.876895.

[11] X. Yang, Z. Long, and Y. Wen, "Investigation of the trade-off between switching losses and EMI generation in Gaussian S-shaping for high-power IGBT switching transients by active voltage control," *IET Power Electron.*, vol. 9, no. 9, pp. 1979–1984, 2016.

[12] X. Yang, Y. Yuan, X. Zhang, and P. R. Palmer, "Shaping high-power IGBT switching transitions by active voltage control for reduced EMI generation," *IEEE Trans. Ind. Appl.*, vol. 51, no. 2, pp. 1669–1677, Mar./Apr. 2015, doi: 10.1109/TIA.2014.2347578.

[13] T. C. Lim, B. W. Williams, S. J. Finney, and P. R. Palmer, "Series-connected IGBTs using active voltage control technique," *IEEE Trans. Power Electron.*, vol. 28, no. 8, pp. 4083–4103, Aug. 2013, doi: 10.1109/TPEL.2012.2227812.
[14] Y. Wang, P. Palmer, T. Lim, S. Finney, and A. Bryant, "Real-time optimization of IGBT/Diode cell switching under active voltage control," in *Proc. Conf. Rec. IEEE Ind. Appl. Conf. 41st IAS Annu. Meeting*, Tampa, FL, UA, Oct. 2006, pp. 2262–2268, doi: 10.1109/IAS.2006.256857.
[15] X. Yang, Y. Yuan, Z. Long, J. Goncalves, and P. R. Palmer, "Robust stability analysis of active voltage control for high-power IGBT switching by Kharitonov's theorem," *IEEE Trans. Power Electron.*, vol. 31, no. 3, pp. 2584–2595, Mar. 2016, doi: 10.1109/TPEL.2015.2439712.
[16] K. Sheng, S. J. Finney, and B. W. Williams, "A new analytical IGBT model with improved electrical characteristics," *IEEE Trans. Power Electron.*, vol. 14, no. 1, pp. 98–107, Jan. 1999, doi: 10.1109/63.737597.
[17] P. R. Palmer, E. Santi, J. L. Hudgins, X. Kang, J. C. Joyce, and P. Yoon Eng, "Circuit simulator models for the diode and IGBT with full temperature dependent features," *IEEE Trans. Power Electron.*, vol. 18, no. 5, pp. 1220–1229, Sep. 2003, doi: 10.1109/TPEL.2003.816194.
[18] A. R. Hefner, "A dynamic electro-thermal model for the IGBT," *IEEE Trans. Ind. Appl.*, vol. 30, no. 2, pp. 394–405, Apr. 1994.
[19] A. R. Hefner and D. M. Diebolt, "An experimentally verified IGBT model implemented in the saber circuit simulator," *IEEE Trans. Power Electron.*, vol. 9, no. 5, pp. 532–542, Sep. 1994, doi: 10.1109/63.321038.
[20] A. R. Hefner, "An improved understanding for the transient operation of the power insulated gate bipolar transistor (IGBT)," *IEEE Trans. Power Electron.*, vol. 5, no. 4, pp. 459–468, Oct. 1990, doi: 10.1109/63.60690.
[21] A. R. Hefner, "Analytical modeling of device-circuit interactions for the power insulated gate bipolar transistor (IGBT)," *IEEE Trans. Ind. Appl.*, vol. 26, no. 6, pp. 995–1005, Nov./Dec. 1990, doi: 10.1109/28.62382.
[22] R. Kraus and H. J. Mattausch, "Status and trends of power semiconductor device models for circuit simulation," *IEEE Trans. Power Electron.*, vol. 13, no. 3, pp. 452–465, May 1998, doi: 10.1109/63.668107.
[23] C. Wong, "EMTP modeling of IGBT dynamic performance for power dissipation estimation," *IEEE Trans. Ind. Appl.*, vol. 33, no. 1, pp. 64–71, Jan./Feb. 1997, doi: 10.1109/28.567078.
[24] A. T. Bryant, L. Lu, E. Santi, J. L. Hudgins, and P. R. Palmer, "Modeling of IGBT resistive and inductive turn-on behavior," *IEEE Trans. Ind. Appl.*, vol. 44, no. 3, pp. 904–914, May/Jun. 2008, doi: 10.1109/TIA.2008.921384.
[25] A. Monti, "A fuzzy-based black-box approach to IGBT modelling," in *Proc. 3rd Int. Conf. Electron., Circuits, Syst.*, Rodos, Greece, vol. 2, 1996, pp. 1147–1150, doi: 10.1109/ICECS.1996.584625.
[26] H. S. Oh and M. E. Nokali, "A new IGBT behavioral model," *Solid State Electronics*, vol. 45, no. 12, pp. 2069–2075, Dec. 2001, doi: 10.1016/S0038-1101(01)00149-6.
[27] J.-T. Hsu and K. D. T. Ngo, "Behavioral modeling of the IGBT using the hammerstein configuration," *IEEE Trans. Power Electron.*, vol. 11, no. 6, pp. 746–754, Nov. 1996, doi: 10.1109/63.542037.
[28] K. Sheng, B. W. Williams, and S. J. Finney, "A review of IGBT models," *IEEE Trans. Power Electron.*, vol. 15, no. 6, pp. 1250–1266, Nov. 2000, doi: 10.1109/63.892840.
[29] Y. Tang and H. Ma, "Dynamic electrothermal model of paralleled IGBT modules with unbalanced stray parameters," *IEEE Trans. Power Electron.*, vol. 32, no. 2, pp. 1385–1399, Feb. 2017, doi: 10.1109/TPEL.2016.2542198.
[30] H. Luo, W. Li, F. Iannuzzo, X. He, and F. Blaabjerg, "Enabling junction temperature estimation via collector-side thermo-sensitive electrical parameters through emitter stray inductance in high-power IGBT modules," *IEEE Trans. Ind. Electron.*, vol. 65, no. 6, pp. 4724–4738, Jun. 2018, doi: 10.1109/TIE.2017.2745442.
[31] X. Yang, J. Zhang, W. He, Z. Long, and P. R. Palmer, "Physical investigation into effective voltage balancing by temporary clamp technique for the series connection of IGBTs," *IEEE Trans. Power Electron.*, vol. 33, no. 1, pp. 248–258, Jan. 2018, doi: 10.1109/TPEL.2017.2673849.
[32] H. Luo, W. Li, and X. He, "Uneven temperature effect evaluation in high-power IGBT inverter legs and relative test platform design," *Microelectron. Rel.*, vols. 76–77, pp. 123–130, Sep. 2017.
[33] L. Zhou, S. Zhou, and M. Xu, "Investigation of gate voltage oscillations in an IGBT module after partial bond wires lift-off," *Microelectron. Rel.*, vol. 53, no. 2, pp. 282–287, Feb. 2013.
[34] A. F. Zahrt, J. J. Henle, B. T. Rose, Y. Wang, W. T. Darrow, and S. E. Denmark, "Prediction of higher-selectivity catalysts by computer-driven workflow and machine learning," *Science*, vol. 363, no. 6424, 2019, Art. no. eaau5631, doi: 10.1126/science.aau5631.
[35] R. Geng, X. Wang, N. Ye, and J. Liu, "A fault prediction algorithm based on rough sets and back propagation neural network for vehicular networks," *IEEE Access*, vol. 6, pp. 74984–74992, 2018, doi: 10.1109/ACCESS.2018.2881890.
[36] L. Tallorin, J. L. Wang, and W. E. Kim, "Discovering de novo peptide substrates for enzymes using machine learning," *Nature Commun.*, vol. 9, no. 5253, pp. 1–10, Dec. 2018.
[37] D. E. Wood, J. R. White, A. Georgiadis, B. Van Emburgh, S. Parpart-Li, J. Mitchell, and S. V. Angiuoli, "A machine learning approach for somatic mutation discovery," *Sci. Transl. Med.*, vol. 10, no. 457, Sep. 2018, Art. no. eaar7939.
[38] X. Zeng, Z. Li, W. Gao, M. Ren, J. Zhang, Z. Li, and B. Zhang, "A novel virtual sensing with artificial neural network and K-means clustering for IGBT current measuring," *IEEE Trans. Ind. Electron.*, vol. 65, no. 9, pp. 7343–7352, Sep. 2018, doi: 10.1109/TIE.2018.2793196.
[39] S. H. Ali, M. Heydarzadeh, S. Dusmez, X. Li, A. S. Kamath, and B. Akin, "Lifetime estimation of discrete IGBT devices based on Gaussian process," *IEEE Trans. Ind. Appl.*, vol. 54, no. 1, pp. 395–403, Jan. 2018, doi: 10.1109/TIA.2017.2753722.
[40] A. Oukaour, B. Tala-Ighil, and B. Pouderoux, "Ageing defect detection on IGBT power modules by artificial training methods based on pattern recognition," *Microelectron. Rel.*, vol. 51, no. 2, pp. 386–391, Feb. 2011.
[41] A. Volke and M. Hornkamp, *IGBT Modules. Technologies, Driver and Application*, 2nd ed. Beijing, China: China Machine Press, 2016, pp. 151–219.
[42] Y. Lobsiger and J. W. Kolar, "Closed-loop di/dt and dv/dt IGBT gate driver," *IEEE Trans. Power Electron.*, vol. 30, no. 6, pp. 3402–3417, Jun. 2015, doi: 10.1109/TPEL.2014.2332811.
[43] C. Y. Sun, X. L. Zhou, and W. Z. Wang, "Description and research review of mind evolutionary computation," in *Proc. 14th China Neural Netw. Academic Conf.*, 2004, pp. 241–251.

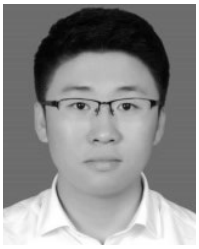

ZHAOLIANG MENG was born in Shaanxi, China, in 1987. He received the B.S. and M.S. degrees from the Xi'an University of Technology, Xi'an, China, in 2010 and 2013, respectively, where he is currently pursuing the Ph.D. degree in circuits and systems.

Since 2013, he has been working with Xi'an Polytechnic University. His research interest includes active gate drive and protection technologies of the high-power IGBTs.

YUAN YANG received the B.S., M.S., and Ph.D. degrees from the Xi'an University of Technology, Xi'an, China, in 1997, 2000, and 2004, respectively. From 2000 to 2004, she was a Lecturer, and from 2004 to 2009, she was an Assistant Professor. Since 2009, she has been working as a Professor with the Department of Electronics, Xi'an University of Technology. In 2005, she was a Visiting Scholar with Kyushu University, Japan. Her research interests include digital-analog mixed integrated circuit designs, the design of track circuit systems, gate drive and protection circuits of the high-power IGBTs, and wide-bandgap semiconductors.

YONG GAO (Member, IEEE) received the B.S. degree in applied physics from the Xi'an University of Technology, Xi'an, China, in 1982, and the M.S. and Ph.D. degrees in microelectronics and solid-state electronics from Xi'an Jiaotong University, Xi'an, China, in 1988 and 1995, respectively. From 1996 to 2009, he was a Professor with the Department of Electronics, Xi'an University of Technology. Since 2010, he has been working as a Professor with the Department of Electronics, Xi'an University of Technology, and the Department of Electrical Engineering, Xi'an Polytechnic University, Xi'an. His research interests include power electronic devices, power integration and integrated circuit designs, and very large-scale integration designs.

SHENGSHENG AI was born in Shaanxi, China, in 1991. He received the B.S. degree from the Baoji University of Arts and Sciences, Baoji, China, in 2015. He is currently pursuing the M.S. degree with Xi'an Polytechnic University, Xi'an, China.

His research interest includes gate drive and protection technologies of SiC MOSFET IPM.

YUE ZHANG received the B.S. and M.S. degrees from the Xi'an University of Technology, Xi'an, China, in 2011 and 2014, respectively.

Since 2014, she has been working with the School of Computer Science, Xi'an Polytechnic University. Her research interests include machine learning and deep learning.

YARU LV was born in Henan, China, in 1994. She received the B.S. degree in electronic information engineering from Luoyang Normal University, China, in 2018. She is currently pursuing the master's degree in electrical engineering with Xi'an Polytechnic University, Xi'an, China.

Her current research interest includes the IGBT junction temperature prediction.

ZETAO ZHANG was born in Gansu, China, in 1995. He received the B.S. degree from the Zhejiang University of Technology, Zhejiang, China. He is currently pursuing the master's degree in electrical engineering with Xi'an Polytechnic University, Xi'an, China.

His current research interest includes machine learning on power electronic device.

YANG WEN was born in Shaanxi, China, in 1990. He received the B.S. and M.S. degrees from Xi'an Polytechnic University, Xi'an, China, in 2012 and 2016, respectively. He is currently pursuing the Ph.D. degree in circuits and systems with the Xi'an University of Technology, Xi'an.

His research interest includes active gate drive and protection technologies of wide-bandgap semi-conductors.

LEI WU was born in Shaanxi, China, in 1984. He received the B.S. and M.S. degrees from the Xi'an University of Technology, Xi'an, China, in 2006 and 2011, respectively, where he is currently pursuing the Ph.D. degree in microelectronics and solid state electronics.

Since 2011, he has been working at CRRC Yongji Electric Company, Ltd. His research interest includes the reliability of high-power IGBTs.

PING ZHANG is currently an Assistant Professor in pattern recognition and intelligence system and data mining. She is also working with the Physics Department, Anshan Normal University, Anshan, China.

JOHN DOUGLAS THOMSON is currently a Senior Lecturer in business with specialisms in e-business, capability delivery, and corporate governance with a strong international profile in performance delivery. He is also working with the Graduate School of Business and Law, RMIT University, Melbourne, VIC, Australia.